

STABILIZED FREE SURFACE FLOWS

Laura Battaglia, Mario A. Storti and Jorge D'Elía

Centro Internacional de Métodos Computacionales en Ingeniería (CIMEC), Instituto de Desarrollo Tecnológico para la Industria Química (INTEC), Universidad Nacional del Litoral - CONICET, Güemes 3450, 3000-Santa Fe, Argentina, e-mail: lbattaglia@ceride.gov.ar (mstorti,jdelia)@intec.unl.edu.ar, web page: <http://www.cimec.org.ar>

Keywords: free surface flows, mesh-movement, finite elements, parallel computing, fluid mechanics, stabilization.

Abstract. In this work, numerical simulations of free surface flows of incompressible and viscous fluids are performed by a finite element computation. As presented in previous works, the free surface movement is followed by a mesh-movement technique (see Battaglia et al, *Mecánica Computacional*, Vol XXIV, pp. 105-116, Buenos Aires, Argentina, Nov. 2005), but because of the fully explicit character of the free surface update equation a smoothing process was used to avoid numerical instabilities. Regarding that the kinematic boundary condition at the interface can be described as a transport-like equation, different authors suggested consistent stabilized finite-element formulations for the free surface, such as streamline upwind/Péetrov-Galerkin (SUPG) (Soulaïmani et al, *Comp. Meth. Appl. Mech. Engrg.*, Vol. 86(3), 1991; Güler et al, *Computational Mechanics*, vol. 23, pp. 117-123, 1999) or Galerkin/Least-Squares (GLS) (Behr et al, *Comp. Meth. Appl. Mech. Engrg.*, Vol. 191(47-48), pp. 5467-5483, Nov. 2002). In this work, a numerical stabilization with this aim is performed as a part of the multi-physics finite element code PETSc-FEM (<http://www.cimec.org.ar/petscfem/>). Numerical examples are shown.

1 INTRODUCTION

As most physical problems, free surface flows are present in many practical situations, as in the sloshing produced in a fluid truck container, the fuel inside a rocket or the flow in a channel. The prediction of the fluid-gas interface position become in such cases an operational data, as maximum wave height, or important design information, regarding the geometry of the container or the profile of the channel.

The main difficulty at the resolution instance is that the free surface position is unknown, because it is part of the solution itself.

Of course, there are many different methods proposed to solve the interface problem, which could be grouped in three categories (Shyy et al., 1996): Lagrangian methods, where the mesh moves with the particles of fluid, Eulerian methods, which count on a fixed mesh and the fluid fills completely the submerged cells or partially the interface ones, and Arbitrary Lagrangian-Eulerian (ALE) methods, that count on meshes whose movement, different from the fluid one, is taken into account at the time of solving the flow field, see Donea and Huerta (2003).

In particular, this work is focused in the resolution of transient free surface problems by a finite element method together with an ALE formulation, where the fluid state is determined by a Navier-Stokes (NS) solver followed by a mesh moving (MMV) one to reach the updated nodal positions, all of them under the scope of the finite element library PETSc-FEM, see Sonzogni et al. (2002) (<http://www.cimec.org.ar/petscfem>).

Besides the modules mentioned, there is a coordinating program which updates the free surface nodal positions by controlling the communication between the NS and the MMV instances each time step. This “free surface updater” (FSU) includes also the resolution of the *kinematic condition* over the interface, that takes the form of an advection equation and consequently could show an unstable behavior when is numerically solved. This fact was already noticed by several authors who appealed to different stabilization methods in order to get satisfactory solutions. Some of these methods are the streamline upwind/Pétrov-Galerkin (SUPG) (Brooks and Hughes, 1982), applied to free surface by Soulaïmani et al. (1991) and Güler et al. (1999), and the Galerkin/Least-Squares (GLS) one, see Behr and Abraham (2002). In this case, the finite element method chosen for updating the free surface is stabilized with SUPG terms for different temporal integration alternatives.

Some examples were solved using the methodology presented, and two of them are presented in this work.

2 GOVERNING EQUATIONS

The procedure adopted for solving free surface consists of the interaction between two main solvers that are part of the PETSc-FEM structure: the first one solves the fluid state, i.e. the Navier-Stokes (NS) solver, and the second one, the mesh movement (MMV) module, determines the updated nodal positions in the domain Ω_t by taking into account the results of the NS one and the free-surface updated position, given by the FSU instance whose objective is to obtain a “stabilized” interface position, which will be described in Sec. 3. The governing equations for the flow and the mesh movement instances are summarized in the following sections.

It is important to notice that PETSc-FEM is a parallel finite element library oriented to multiphysics, based on the Message Passing Interface (Message Passing Interface (MPI), 2006) and the Portable Extensible Toolkit for Scientific Computation (PETSc) (Balay et al., 2005).

2.1 Flow Field

The flow field is represented by the NS equations, which are solved by the corresponding Finite Element (FE) solver under the PETSc-FEM scope and are given by

$$\begin{aligned} \rho(\partial_t \mathbf{v} + \mathbf{v} \cdot \nabla \mathbf{v} - \mathbf{f}) - \nabla \cdot \boldsymbol{\sigma} &= 0 ; \\ \nabla \cdot \mathbf{v} &= 0 ; \end{aligned} \quad (1)$$

over the flow domain $\Omega_t = \Omega(t)$ at time $t \in [0, T]$, being \mathbf{v} the fluid velocity, \mathbf{f} the body force, ρ the fluid density, T a final time and ∂_t indicates the temporal partial derivative. The tensor $\boldsymbol{\sigma}$ is the fluid stress one, and can be decomposed into an isotropic $-p\mathbf{I}$ and a deviatoric part \mathbf{T} ,

$$\boldsymbol{\sigma} = -p\mathbf{I} + \mathbf{T} ; \quad (2)$$

where p is the pressure, \mathbf{I} the identity tensor and \mathbf{T} is related linearly with the strain rate tensor $\boldsymbol{\epsilon}$ because only Newtonian fluids are considered, that is,

$$\mathbf{T} = 2\mu\boldsymbol{\epsilon} ; \quad \boldsymbol{\epsilon} = \frac{1}{2} \left[\nabla \mathbf{v} + (\nabla \mathbf{v})^T \right] ; \quad (3)$$

with μ and $\nu = \mu/\rho$ the dynamic and kinematic viscosities of the fluid, respectively. Here, $(\dots)^T$ indicates transposition. The boundary conditions at the domain boundaries Γ are such as

$$\begin{aligned} \mathbf{v} &= \mathbf{v}_{wall} \text{ at } \Gamma_{wall} ; \\ \boldsymbol{\sigma} \cdot \mathbf{n} &= \mathbf{t} \quad \text{at } \Gamma_t ; \end{aligned} \quad (4)$$

where Γ_{wall} represents the solid boundaries, whose velocity can be null or not, according to the kinematic of the domain, and Γ_t is a traction surface or interface between two fluids, where traction forces \mathbf{t} act. In the case of free surfaces, the gas-phase viscosity is negligible, as well as its density, then on the gas side the parameters are

$$\begin{aligned} p &= P_{atm} \text{ at } \Gamma_{FS} ; \\ \boldsymbol{\tau} \cdot \mathbf{n} &= 0 \quad \text{at } \Gamma_{FS} ; \end{aligned} \quad (5)$$

being Γ_{FS} the free surface, P_{atm} the pressure exerted by the gas-phase, usually the atmospheric one, and $\boldsymbol{\tau}$ the tangential stresses exerted by the gas over the liquid surface. Notice that from last expression of Eq. (5) that the free surface is allowed to move only along its normal direction, and that the traction forces result $\mathbf{t} = -P_{atm} \mathbf{n}$, or

$$\boldsymbol{\sigma} \cdot \mathbf{n} = -P_{atm} \mathbf{n} \text{ at } \Gamma_{FS}. \quad (6)$$

In this way, the complete set of data is given if a weak formulation of the Divergence Form of the NS equations (Limache and Idelsohn, 2006) is chosen for solving the problem, as made here. It is worth to mention that in the case of $P_{atm} = 0$, as is usually made, the boundary term over Γ_{FS} disappears, being unnecessary any pressure imposition over this boundary.

This system of partial differential equations is discretized by a finite element method in space, giving an ordinary differential equations system in time. The last one is discretized by a finite difference method in an implicit way, expressed as

$$\mathbf{F} \left(\frac{\mathbf{v}^{n+1} - \mathbf{v}^n}{\Delta t}, \mathbf{p}^{n+1} \right) = \mathbf{0} ; \quad (7)$$

giving the flow field at time t^{n+1} from the state at $t = t^n$.

2.2 Mesh Update

Once the fluid state is solved, the positions of the internal nodes are updated through one of two available strategies for mesh movement. Both of them require as incoming data the free surface displacement, which is determined by the process described in Sec. 3, and keeping the topology of the mesh unchanged.

The mesh updating strategies, which are also detailed in previous works as Battaglia et al. (2006b), are summarized as follows.

2.2.1 Pseudo-elastic mesh update

The mesh update process consists of the resolution of a pseudo-elastic problem over the initial domain Ω_0 with Dirichlet boundary conditions.

The formulation applied is a standard one,

$$\begin{aligned}\sigma_{ij,j} &= 0 ; \\ \sigma_{ij} &= 2\tilde{\mu}\epsilon_{ij} + \tilde{\lambda}\delta_{ij}\epsilon_{kk} ; \\ \epsilon_{ij} &= \frac{1}{2}(u_{i,j} + u_{j,i}) ;\end{aligned}\tag{8}$$

with δ_{ij} as the Kronecker tensor and the Lamé elastic constants, $\tilde{\mu}$ and $\tilde{\lambda}$, for the fictitious material, although in practice the pseudo parameters Poisson ratio $\tilde{\nu}$ and elasticity modulus \tilde{E} are used. The first one set to $\tilde{\mu} = 0.3$, and as there are only Dirichlet boundary conditions, the displacements are independent of a multiplicative constant in the elasticity modulus, so it is usually $\tilde{E} = 1$, but in some special cases a variable \tilde{E} is used over the domain in order to reduce mesh distortions, like in sectors with closed corners.

The boundary conditions over the free surface are computed as $\mathbf{u}_j = \mathbf{x}_j^{n+1} - \mathbf{x}_j^0$, where \mathbf{u} represents the nodal displacements and \mathbf{x}_j^n the position of node x_j at the time step n , whereas for solid walls or the fluid domain limits the slip or non-slip conditions, $\mathbf{u} \cdot \hat{\mathbf{n}} = 0$ and $\mathbf{u} = 0$ respectively, are adopted.

The pseudo-elastic problem can be considered linear or non-linear, proposing an elemental stiffness matrix \mathbf{K}_e according to Xu and Accorsi (2004),

$$\mathbf{K}_e = \int_{\Omega_t^e} \mathbf{B}^T \mathbf{D} \mathbf{B} |\mathbf{J}|^e \kappa^e d\Omega_t^e ;\tag{9}$$

where the matrix \mathbf{B} contains the shape functions derivatives, \mathbf{D} is the constitutive matrix, $|\mathbf{J}|^e$ is the elemental Jacobian and κ^e controls the stiffening and is calculated as

$$\kappa^e = \left(\frac{|\mathbf{J}|^0}{|\mathbf{J}|^e} \right)^s ;\tag{10}$$

with the arbitrary chosen stiffness exponent s and $|\mathbf{J}|^0$ as a coefficient needed for consistency. If $s = 0$, the problem solved is a linear elastic one, whereas for a non-linear alternative $s > 0$ is used, making the smaller elements more stiffened than the larger ones, and being $s < 0$ inconvenient for the purpose of the method, see Tezduyar et al. (1993) and Stein et al. (2004).

2.2.2 Mesh motion by a mesh-quality optimization

Although this mesh motion method is used here for following the nodal displacements induced by the free surface movement, this method was proposed for moving boundary problems in general, see López et al. (2007). It consists of the resolution of an optimization problem where the objective is minimizing a functional written over the set of mesh coordinates $\{x_j^\alpha\}$ as

$$F = F(\{x_j^\alpha\}); \quad (11)$$

being x_j^α is α -coordinate of j -node. As there are some specific requirements over F demanded by the minimization process, it is proposed as a sum of elemental contributions,

$$F = \sum_e F_e; \quad F_e = C_v \left(\frac{V_e}{V_{ref}} - 1 \right)^m + C_Q Q^n; \quad (12)$$

where V_e is the volume of the element e , V_{ref} is the reference volume, C_v and C_Q are user-chosen weight coefficients, m and n norms for size and shape terms and Q is a quality parameter calculated as

$$Q = \frac{C V_e}{\sum_i l_i^p}; \quad (13)$$

with l_i the length of each edge length of the element, weighted to the power p which corresponds to the space dimension. Finally, the constant C is determined in order to get $0 < Q \leq 1$, where $Q = 1$ corresponds to equilateral elements, being $C = 4\sqrt{3}$ for triangles and $C = 36\sqrt{2}$ for tetrahedrons.

3 FREE SURFACE TREATMENT

The free surface nodal displacements are chosen to be constrained along a given direction \hat{s}_j , which is fixed during the whole study, giving the new free surface position of j -node in time t as

$$\mathbf{x}_j(t) = \mathbf{x}_{0,j} + \eta_j(t) \hat{s}_j; \quad (14)$$

where the fixed direction or “spine” is \hat{s}_j , $\mathbf{x}_{0,j}$ is the initial position of node j and η_j is the scalar coordinate, all of them indicated in Fig. 1. Usually, \hat{s}_j is normal to the free surface at rest of the problem to be solved.

An important remark is that the spines are used only for the displacement of the free surface, and inside the domain the nodal positions are determined by one of the methods presented in Sec. 2.2. In this way, mesh distortion is reduced in comparison with cases where all the nodes move over fixed spines.

3.1 Equation of Movement

The free surface movement is ruled by the so-called *kinematic condition*. This condition takes the physical meaning of a material interface, where there is no material exchange, see Behr and Abraham (2002) or García Espinosa (1999), and can be expressed as

$$\mathbf{v} \cdot \mathbf{n} = \frac{\partial \eta}{\partial t} \cdot \mathbf{n} \quad \text{over } \Gamma_{FS}; \quad (15)$$

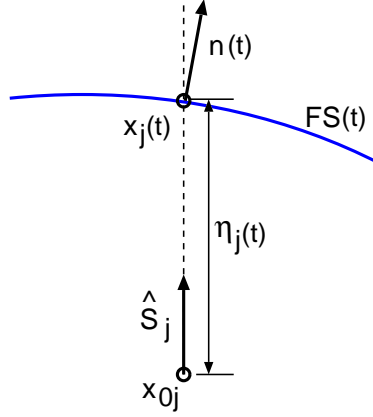


Figure 1: Free surface nodal displacements.

where \mathbf{n} is the free-surface normal direction and $\boldsymbol{\eta}$ is the displacement of the interface over the spine direction $\hat{\mathbf{s}}$, $\boldsymbol{\eta} = \eta \hat{\mathbf{s}}$, with η the scalar displacement, see Fig. 1. Replacing in Eq. (15),

$$\frac{\partial \eta}{\partial t} = \frac{\mathbf{v} \cdot \mathbf{n}}{\hat{\mathbf{s}} \cdot \mathbf{n}}. \quad (16)$$

Notice that relevant displacements are those normal to the free surface, while the tangential ones can be neglected.

Regarding Eq. (14) and the scalar field $\eta = \eta(x_1, x_2, t)$ for the three-dimensional case, the free surface can be expressed as $F(\mathbf{x}) = x_3 - \eta = 0$, and its normal vector is determined as the gradient, taken as

$$\mathbf{n} = \nabla F(\mathbf{x}) = \left[-\frac{\partial(\eta \hat{s}_1)}{\partial x_1}; -\frac{\partial(\eta \hat{s}_2)}{\partial x_2}; 1 \right]^T; \quad (17)$$

By replacing in Eq. (16) with (17) and introducing $H = \hat{\mathbf{s}} \cdot \mathbf{n}$,

$$\frac{\partial \eta}{\partial t} = \frac{1}{H} \mathbf{v} \cdot \mathbf{n} = \frac{1}{H} \left[-v_1 \frac{\partial(\eta \hat{s}_1)}{\partial x_1} - v_2 \frac{\partial(\eta \hat{s}_2)}{\partial x_2} + v_3 \right]; \quad (18)$$

giving the expression for η as an advection equation. The reduction for two-dimensional (2D) free surface flows is immediate.

From Eq. (18), and considering that for small deformations of the free surface \mathbf{n} is nearly vertical and $\hat{\mathbf{s}} = \hat{\mathbf{e}}_3$, being $\hat{\mathbf{e}}_3$ the coordinate unit vector corresponding to the vertical axis adopted, then $H = \hat{\mathbf{s}} \cdot \mathbf{n} \approx 1$.

In order to maintain a uniform notation in following expressions, and for giving a clearer formulation, the problem to solve is written as the advective system,

$$\begin{aligned} \frac{\partial \eta}{\partial t} + \mathbf{v}_{\parallel} \cdot \hat{\nabla} \eta &= s \quad \text{in } \Omega'_{FS}; \\ \eta &= \eta_D \quad \text{over } \Gamma'_D; \end{aligned} \quad (19)$$

being $\mathbf{v}_{\parallel} = [v_1; v_2]^T$ the tangential velocity vector, $\hat{\nabla} \eta = [\frac{\partial \eta}{\partial x_1}; \frac{\partial \eta}{\partial x_2}]^T$ the two-dimensional gradient of η and $s = v_3$ the source term given by the velocity of the fluid in vertical direction at each point of the free surface, i.e. over the normal to the interface. Besides, $\Omega'_{FS} = \Gamma_{FS}$ in Eq. (5) is the $n_{\text{dim}} - 1$ interface domain, corresponding to a n_{dim} flow problem with a free surface, and Γ'_D is the boundary Dirichlet condition for the advection equation given. As Eq. (19) represents a hyperbolic problem, Γ'_D is the inflow boundary, where $\mathbf{v}_{\parallel} \cdot \hat{\mathbf{n}} < 0$ is verified, with $\hat{\mathbf{n}} = [n_1; n_2]^T$.

3.2 Numerical Stabilization

As mentioned in the Introduction, other authors already reported that the free surface kinematic condition is a transport-like equation that shows numerical instabilities under certain conditions such as high convective velocity. In order to improve results, there are some “classic” stabilization methods that have been applied to free surface displacements, which are the SUPG (see again [Soulaïmani et al. \(1991\)](#) or [Güler et al. \(1999\)](#)) and the GLS ([Behr and Abraham, 2002](#)) ones.

In previous works, like [Battaglia et al. \(2006a\)](#), the free surface stabilization was made through a smoothing operator based on solving a pseudo-heat problem over the free surface with artificial parameters. This procedure is appropriate for low velocities and deformations, but as the mean values of these fields grows, results become unstable or show important differences when they are compared to analytical or semi-analytical solutions.

The SUPG method, introduced in [Brooks and Hughes \(1982\)](#), was chosen to be applied over the NS solver results, i.e. before the mesh update process, for determining the free surface nodal positions for the next time step. The variational formulation followed was taken from [Donea and Huerta \(2003\)](#), and is based on the functional spaces $\mathcal{S} := \{\eta \in H^1(\Omega'_{FS}) | \eta = \eta_D \text{ over } \Gamma'_D\}$ and $\mathcal{W} := \{w \in H^1(\Omega'_{FS}) | w = 0 \text{ over } \Gamma'_D\}$. The problem statement is *find* $\eta \in \mathcal{S}$ such that

$$\int_{\Omega'_{FS}} w \frac{\partial \eta}{\partial t} d\Omega'_{FS} + \int_{\Omega'_{FS}} w (\mathbf{v}_{\parallel} \cdot \hat{\nabla} \eta) d\Omega'_{FS} = \int_{\Omega'_{FS}} w s d\Omega'_{FS}; \quad (20)$$

or expressed in compact form,

$$a(w, \eta) + c(\mathbf{v}_{\parallel}; w, \eta) = (w, s) \text{ in } \Omega'_{FS}; \quad (21)$$

where the terms are identified with the former expression as follows,

$$\begin{aligned} a(w, \eta) &= \int_{\Omega'_{FS}} w \frac{\partial \eta}{\partial t} d\Omega'_{FS}; \\ c(\mathbf{v}_{\parallel}; w, \eta) &= \int_{\Omega'_{FS}} w (\mathbf{v}_{\parallel} \cdot \hat{\nabla} \eta) d\Omega'_{FS}; \\ (w, s) &= \int_{\Omega'_{FS}} w s d\Omega'_{FS}. \end{aligned} \quad (22)$$

A *consistent* stabilization over the formulation given in Eq. (21) can be written like

$$a(w, \eta) + c(\mathbf{v}_{\parallel}; w, \eta) + \sum_e \int_{\Omega'_e} \mathcal{P}(w) \tau_S \mathcal{R}(\eta) d\Omega'_e = (w, s) \text{ in } \Omega'_{FS}; \quad (23)$$

with τ_S the intrinsic time or stabilization parameter, described later in this section, Ω'_e indicates that integration is carried out over each element, the residual of the differential equation calculated as

$$\mathcal{R}(\eta) = \frac{\partial \eta}{\partial t} + \mathbf{v}_{\parallel} \cdot \hat{\nabla} \eta - s = \mathcal{L}(\eta) - s; \quad (24)$$

and the operator $\mathcal{P}(w)$, which in the case of SUPG stabilization is

$$\mathcal{P}(w) = \mathbf{v}_{\parallel} \cdot \hat{\nabla} w. \quad (25)$$

The resulting discrete problem takes the form of *find* $\eta^h \in \mathcal{S}^h$ such that

$$a(w^h, \eta^h) + c(\mathbf{v}_{\parallel}; w^h, \eta^h) + \sum_e \int_{\Omega'_e} \mathcal{P}(w^h) \tau_S \mathcal{R}(\eta^h) d\Omega'_e = (w^h, s); \quad (26)$$

for all $w^h \in \mathcal{W}^h$, with $\eta^h \in \mathcal{S}^h$, being \mathcal{W}^h and \mathcal{S}^h subspaces of finite dimension of \mathcal{W} and \mathcal{S} , respectively.

The intrinsic time τ_S is taken as

$$\tau_S = \frac{h}{2\|\mathbf{a}\|}; \quad (27)$$

where h is a characteristic element size and \mathbf{a} is a mean velocity at each element, considering that there is a velocity field with, in general, different values of $\mathbf{v}_{parallel}$ for different nodes.

3.3 Implementation

The FEM implementation of the free surface stabilization for a 2D flow problem implies that the advective system is one-dimensional (1D). Then, while the NS problem and the MMV instance are solved over quadrangular elements, the interface is discretized by 2-node linear elements for solving Eq. (26), but considering now that the vertical axis has x_2 -direction, i.e. for $\mathbf{v} = [v_1; v_2]^T$ the velocities in the advection problem are $\mathbf{v}_{\parallel} = v_1$ and $s = v_2$.

Replacing in Eqs. (24) to (26), the problem become *find* $\eta^h \in \mathcal{S}_{FS}^h$ such that

$$a(w^h, \eta^h) + c(v_1; w^h, \eta^h) + \sum_e \int_{\Omega'_e} \left(v_1 \frac{\partial w^h}{\partial x_1} \right) \tau_S^e \left(\frac{\partial \eta^h}{\partial t} + v_1 \frac{\partial \eta^h}{\partial x_1} - v_2 \right) d\Omega'_e = (w^h, v_2); \quad (28)$$

for all $w^h \in \mathcal{W}_{FS}^h$, with $\eta^h \in \mathcal{S}_{FS}^h$, being \mathcal{W}_{FS}^h and \mathcal{S}_{FS}^h subspaces of finite dimension of \mathcal{W}_{FS} and \mathcal{S}_{FS} , the functional spaces corresponding to \mathcal{W} and \mathcal{S} from Sec. 3.2 for 1D problems, respectively.

The intrinsic time $\tau_S^e = h(2a)^{-1}$ is calculated for each element, taking in account that h is the length of the element considered and a the arithmetic mean between the nodal velocities in x_1 -direction.

The matrix form of Eq. (28) after the elemental assembly is:

$$(\mathbf{M} + \mathbf{C}_S) \boldsymbol{\eta}_t + (\mathbf{C} + \mathbf{K}_S) \boldsymbol{\eta} = (\mathbf{M} + \mathbf{C}_S) \mathbf{s}; \quad (29)$$

where \mathbf{M} and \mathbf{C} are the mass and the convection matrices, respectively, \mathbf{C}_S and \mathbf{K}_S are the pseudo-convection and pseudo-diffusion matrices which arise from integration of stabilization terms. All the matrices count on $n_{\text{nod}_{FS}} \times n_{\text{nod}_{FS}}$ elements, being $n_{\text{nod}_{FS}}$ the number of free surface nodes, which is the same as the quantity of the unknowns. The vector \mathbf{s} groups the $n_{\text{nod}_{FS}}$ ‘‘source’’ terms given by the vertical velocity components v_2 , $\boldsymbol{\eta}$ is the vector of unknowns and $\boldsymbol{\eta}_t$ is the vector of temporal partial derivatives of $\boldsymbol{\eta}$.

The temporal integration is made through a ‘‘ θ family of methods’’ which requires a reformulation of Eqs. (28) and (29), and taking into account that $\boldsymbol{\eta}_t = (\boldsymbol{\eta}^{n+1} - \boldsymbol{\eta}^n)/\Delta t$, the system of equations to be solved looks like the following,

$$\begin{aligned} & [\mathbf{M} + \mathbf{C}_S^{n+1} + \theta \Delta t (\mathbf{C}^{n+1} + \mathbf{K}_S^{n+1})] \boldsymbol{\eta}^{n+1} \\ & = (\mathbf{M} + \mathbf{C}_S^{n+1}) [\theta \Delta t \mathbf{s}^{n+1} + (1 - \theta) \Delta t \mathbf{s}^n + \boldsymbol{\eta}^n] - (1 - \theta) \Delta t (\mathbf{C}^{n+1} + \mathbf{K}_S^{n+1}) \boldsymbol{\eta}^n; \end{aligned} \quad (30)$$

where the value of θ leads to different methods, being $\theta = 1$ for Backward-Euler, $\theta = 0$ for the classic Euler, and $\theta = 0.5$ for Crank-Nicolson. Regarding the unconditional stability of methods with $\theta \geq 0.5$, all the problems are solved with θ inside this interval.

After some tests, especially those where velocities were relatively important, it was necessary the incorporation of a prediction step for both the NS and the MMV instances, in order to count on an updated fluid state at the time of computing the updated nodal positions over the mesh.

The system of Eq. (30) is solved inside a “hook”, which is a C program that, in this case, communicates the NS instance with the MMV one and uses PETSc (Balay et al., 2005) iterative routines for solving the linear system of equations. In this way, the hook is prepared to be used for parallel computations.

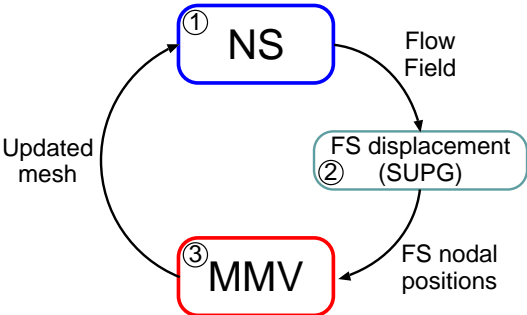


Figure 2: Sequence of execution of the different instances involved in free surface problems.

A graphic representation of the scheme implemented can be appreciated in Figs. 2 and 3. The first of them shows the simplest case, where the NS solver determines the flow field, then the free surface nodal displacements are calculated and, at the end of each time step, the nodal positions for the whole mesh are updated through the MMV process. The second figure shows the order of execution of each part of the system when there is a prediction loop with a user-chosen quantity of time steps “p”. The difference consist of the determination of the fluid state for a global step over a predicted mesh, which was found after the interaction of two auxiliar NS and MMV processes. This auxiliar prediction part of the resolution leads to more precise results from the main instances, indicated with numbers 2 and 4 in the graphic.

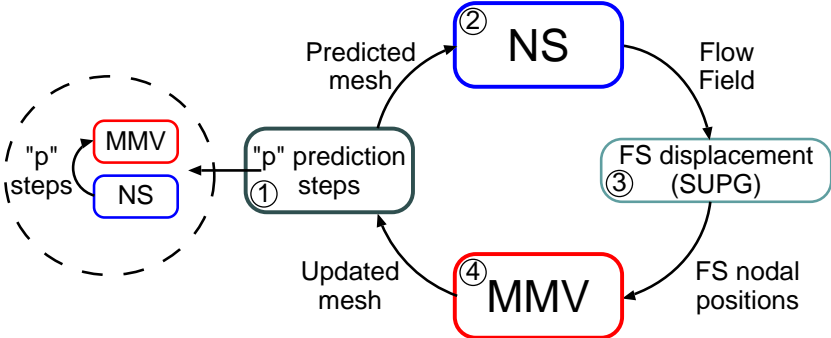


Figure 3: Sequence of execution of the different instances for free surface problems with prediction instance.

4 NUMERICAL EXAMPLES

4.1 Viscous free surface flow with periodic boundary conditions

The free surface position in a two-dimensional (2D) incompressible viscous fluid with a given initial deformation over the interface is known for the case of infinite depth and lateral extent, see Prosperetti (1981). The problem consist of a small-amplitude wave as initial condition which evolves in time, being damped by the fluid viscosity.

The simulation was performed over a domain of height H and width L , see Fig. 4, being a_0 the initial amplitude of the motion, which is negligible compared to the depth H . The infinite lateral domain is taken in account with periodic boundary conditions over the laterals, with a wave length of L . The perfect slip condition is imposed over the bottom of the domain, considering that the superficial perturbations are small and does not modify the flow there. There are also a gravity acceleration g applied and a kinematic viscosity ν involved.

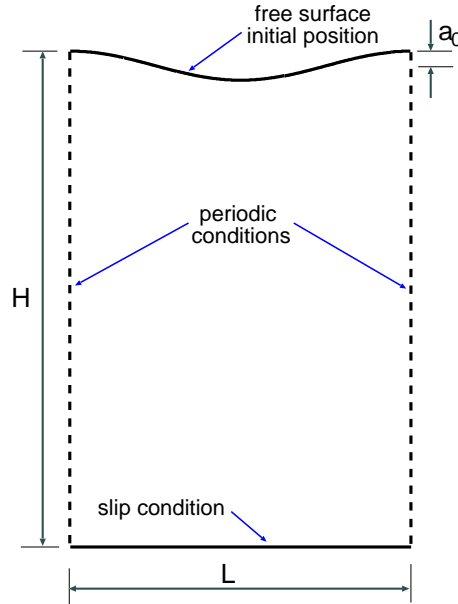


Figure 4: Geometrical data and boundary conditions for the waves with periodic flow.

The initial free surface profile is given by

$$h(x) = 1.5 + a_0 \cos(2\pi x) . \quad (31)$$

In the linearized case, the analytical solution describing the vertical movement of one point of the free surface as a function of time t is

$$a(t) = \frac{4\nu^2 k^4}{8\nu^2 k^4 + \omega_0^2} a_0 \operatorname{erfc}(\nu k^2 t)^{1/2} + \sum_{i=1}^4 \frac{z_i}{Z_i} \left(\frac{\omega_0^2 a_0}{z_i^2 - \nu k^2} \right) \exp[(z_i^2 - \nu k^2)t] \operatorname{erfc}(z_i t^{1/2}) ; \quad (32)$$

with k the wave number, $\omega_0^2 = gk$ the inviscid natural frequency, and each z_i a root of the following algebraic equation,

$$z^4 + k^2 \nu z^2 + 4(k^2 \nu)^{3/2} z + \nu^2 k^4 + \omega_0^2 = 0 ; \quad (33)$$

being $Z_1 = (z_2 - z_1)(z_3 - z_1)(z_4 - z_1)$ and Z_2, Z_3, Z_4 obtained by circular permutation of the indices. Finally, $\operatorname{erfc}(\dots)$ is the error function for complex variable. This expression is valid for small-amplitude flat waves in an infinite depth domain.

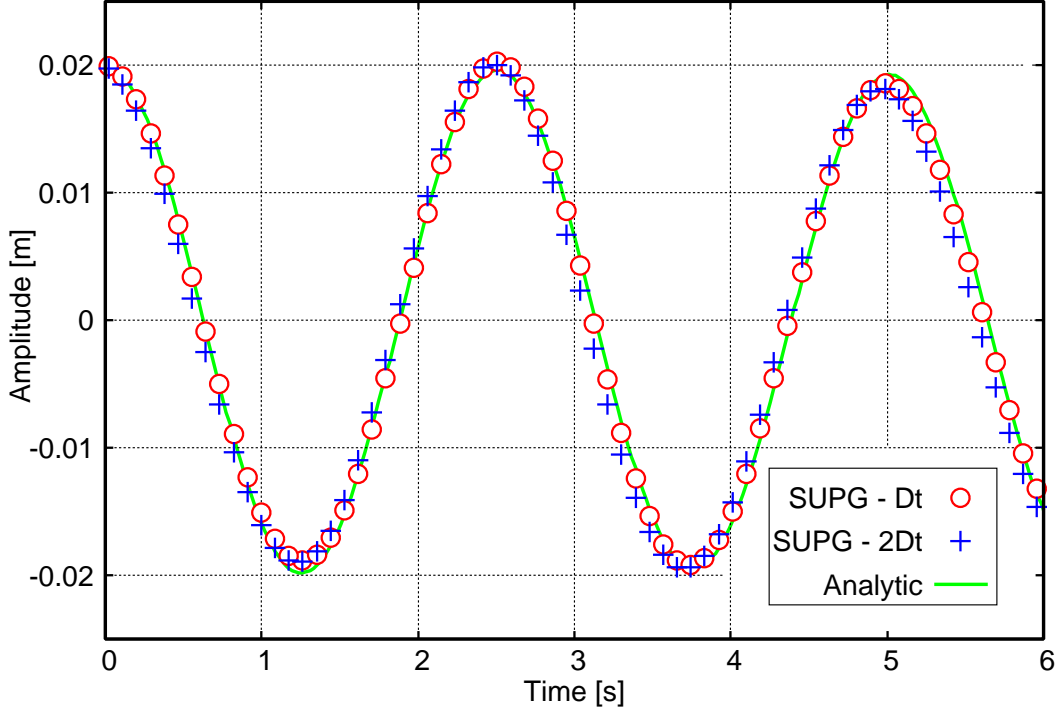


Figure 5: Vertical displacement of the left node of the free surface.

The set of data used for the numerical resolution is $H = 1.50$ m, $L = 1.00$ m, $a_0 = 0.02$ m, with $p = P_{\text{atm}}$ and $\boldsymbol{\tau} \cdot \mathbf{n} = 0$ over the surface, $g = 1$ m/s², together with density $\rho = 1$ kg/m³ and kinematic viscosity $\nu = 0.0001$ m²/s as the fluid characteristics. The problem was solved until $t \approx 6$ s, with a time steps $\Delta t = T/80 = 0.022$ s and $\Delta t' = 2\Delta t$, with T an estimation of the period of the wave imposed as initial position of the free surface. The spatial discretization counts on 40×60 quadrangular elements with equal sides, being 40 the free surface elements.

The free surface left node takes different vertical positions as the time evolves, describing a curve plotted in Fig. 5, where there are also shown the numerical results, as crosses for $\Delta t = T/40$ and dots in the case $\Delta t = T/80$. In this figure, it is possible to see that the numerical solution converges to the analytic one as Δt diminishes, showing the consistency of the method.

4.2 Rectangular container submitted to horizontal periodic acceleration

This example consist of the simulation of large amplitude sloshing inside a tank generated by a horizontal acceleration whose value is periodic in time. The problem was first proposed by Huerta and Liu (1988) and reproduced by Soulaïmani et al. (1991). In spite of the formulation considered in the present work, focused on small free surface displacements, this examples shows how robust is the method at the time of solving large displacements and horizontal velocities higher than those determined in the problem of Sec. 4.1.

The tank is a rectangular container of width $W = 0.80$ m with water height $D = 0.30$ m, as shown in Fig. 6, which is modelled as a 2D problem. As this fluid counts on a low kinematic viscosity of $\nu = 1.0 \times 10^{-6}$ m²/s, perfect slip boundary conditions are taken over the walls.

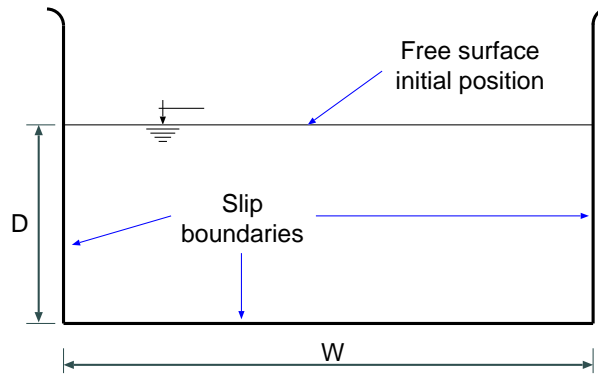


Figure 6: Geometrical data and boundary conditions for the horizontally accelerated container.

The acceleration over the domain is $G = [g_1, g_2]^T$, being the vertical component $g_2 = -g = -9.81 \text{ m/s}^2$ and the horizontal one $g_1 = A g \sin \omega t$, where the coefficient of amplitude is $A = 0.01$, t is the time and ω the circular frequency. This frequency was calculated in such a way that the first sloshing mode is excited, considering that the wavelength is $\lambda = 2W$, that is,

$$f = \sqrt{\frac{g}{4\pi W} \tanh \frac{\pi D}{W}} = 0.89825 \text{ 1/s} . \quad (34)$$

Then, the circular frequency to be imposed is $\omega = 2\pi f = 5.64 \text{ rad/s}$.

This problem was solved for several mesh discretizations and different time steps, using Crank-Nicolson and Backward Euler for temporal integration, and performing one or more prediction steps before each time step. Results are plotted in Figs. 7 to 9.

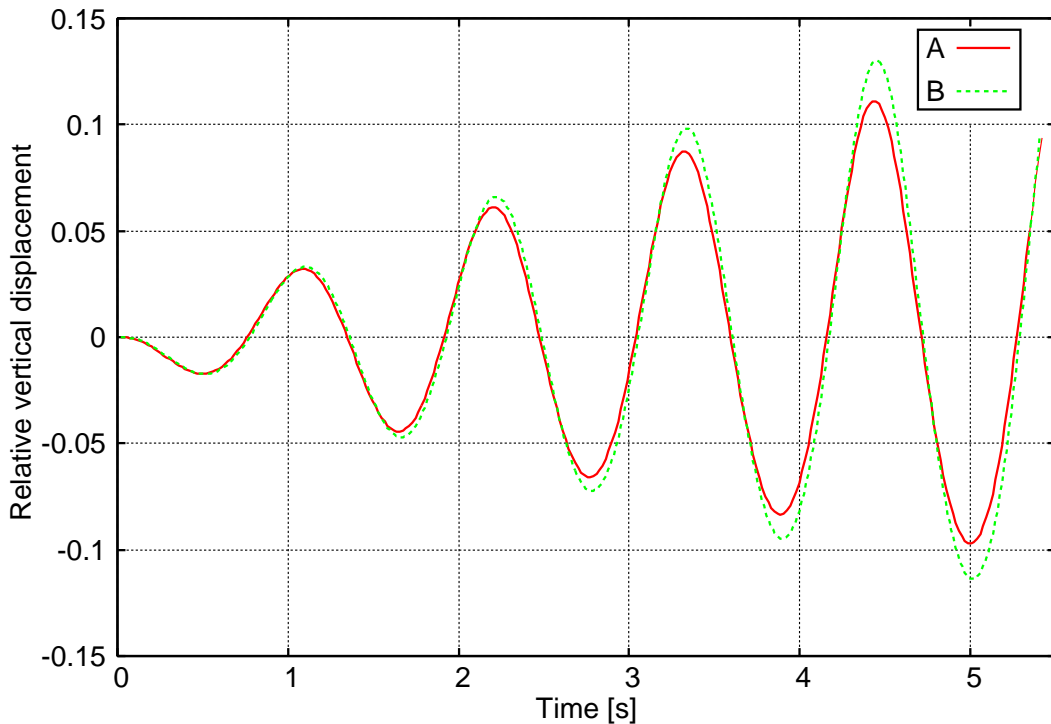


Figure 7: Vertical displacements for the left free surface node relative to the container depth, with $\Delta t = 0.018 \text{ s}$ for “A” and $\Delta t = 0.009 \text{ s}$ for “B”

First, the problem was solved for different mesh refinement, in this case for 60×160 and 54×144 quad elements, showing small differences among the results achieved, under $\mathcal{O}(10^{-5})$ in the case of free surface displacements relative to D . The time step was also modified, proving that the free surface displacements are much sensitive to this parameter, as shown in Figs. 7 and 8, where both the “A” and “B” tests were solved with a 2D mesh of 54×144 quads, with $\Delta t = 0.018s$ for the first and $\Delta t = 0.009s$ for the last one.

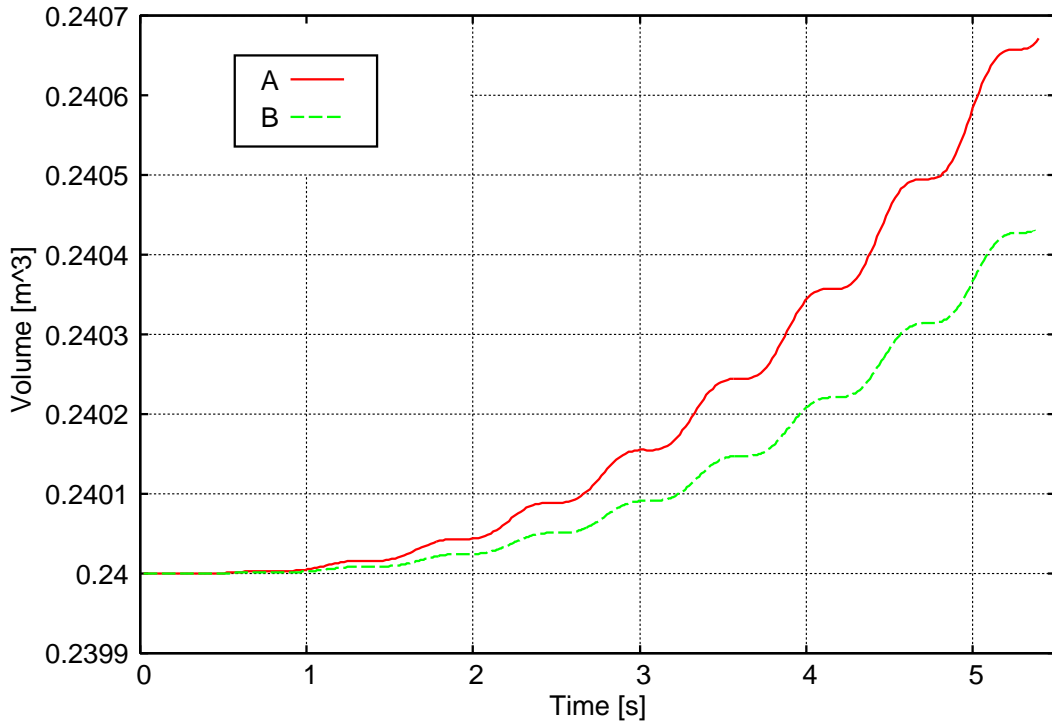


Figure 8: Evolution of the volume of fluid inside the container, taking $\Delta t = 0.018$ s for the example “A” and $\Delta t = 0.009$ s for the “B” one.

The use of different temporal integration schemes, as plotted in Fig. 9 for a 39×104 elements mesh solved with $\Delta t = 0.009$ s, shows the evolution of the left node displacement during 2000 time steps. Taking into account that the container is excited with the frequency of the first sloshing mode, the permanent increase in the amplitude of the movement is expected, that would indicate that $\theta = 0.5$ gives a more appropriate temporal integration. In this case, for $\theta = 0.5$ the volume was increased in less than 4%, while for $\theta = 1.0$ the increment is practically negligible.

4.3 Supercritical flow over a bump

In this case, a supercritical flow in a channel with a parabolic bottom obstruction, called “bump”, is simulated as another example for testing the developed stabilization procedure. For the viscous fluid case, neither (semi)-analytic solutions nor experimental results were available for the range of parameters considered, but potential analytic solutions such as those proposed by Forbes and Schwartz (1982) for semicircular bumps are taken as reference for the computational results. These potential results indicate that the free surface position for a supercritical flow over an obstruction is a symmetric curve, centered with its vertical axis and situated above the interface position at rest.

The geometry of the domain is presented in Fig. 10, as well as the references for the boundary conditions and the free surface initial position. Dimensions are $H_c = 1.00$ m as the initial

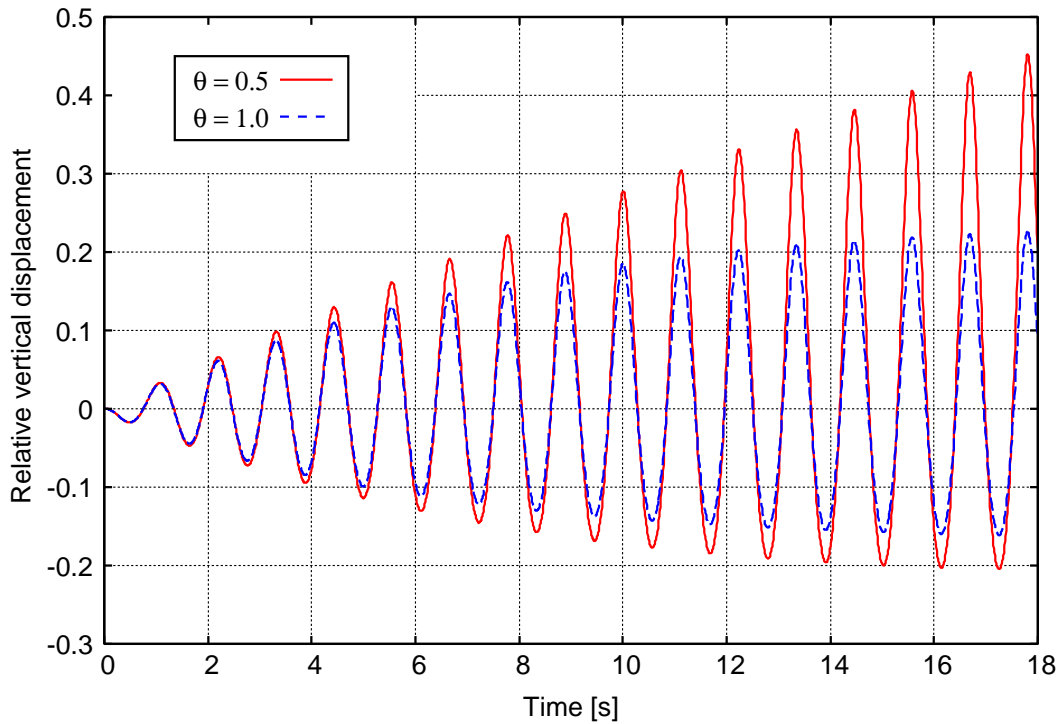


Figure 9: Vertical displacement of the left node of the free surface relative to the depth of the tank for different temporal integration parameters.

deep of the fluid, up-water and down waters lengths are respectively $L_u = 3.00$ m and $L_d = 5.00$ m, while the bump has a parabolic profile of $H_b = 0.50$ m height and $L_b = 1.00$ m width. Conditions imposed over the boundaries for the NS problem are given as follows: for the free surface, number (1) in the figure, the traction free condition is used, the perfect slip one is considered over the bottom (3), the outlet section is free (4), i.e. there is no condition applied, and for the inlet section (2) the horizontal velocity is set to $v_{in} = 1.50$ m/s. In the case of the MMV instance, carried out with the method described in Sec. 2.2.1, all the nodes of (3) are fixed, while the inlet (2) and outlet sections (4) have null horizontal displacements and the movement of the nodes over the free surface (1) is the result of the updating routine between the NS and the MMV modules. Besides, vertical displacements over (2) are prevented because of the supercritical condition of the flow, which means that all the data for the problem should be fixed over the inlet section, which in this case consist of the incoming velocity and the height of the section considered.

Finally, the fluid with kinematic viscosity $\nu = 0.005$ m²/s and density $\rho = 1$ kg/m³ is submitted to a gravitational field of $g = 1$ m/s² in the negative vertical direction. These data

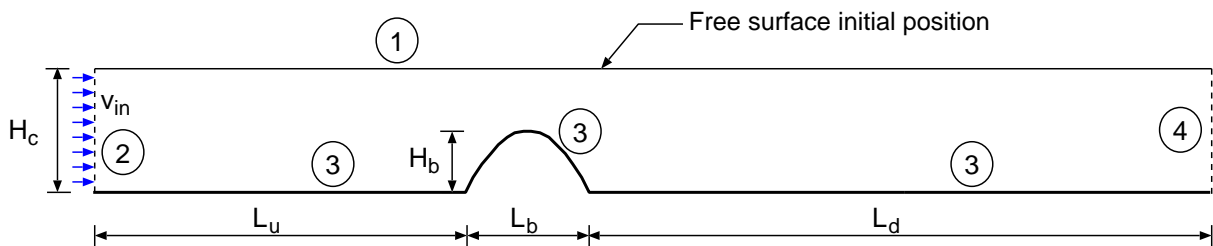


Figure 10: Geometry and references for the channel with supercritical flow over a bottom obstruction.

leads to a Froude number of $Fr = 1.50$ and a Reynolds number of $Re \approx 300$, indicating that the flow is supercritical and that no turbulence should be taken into account for the numerical resolution.

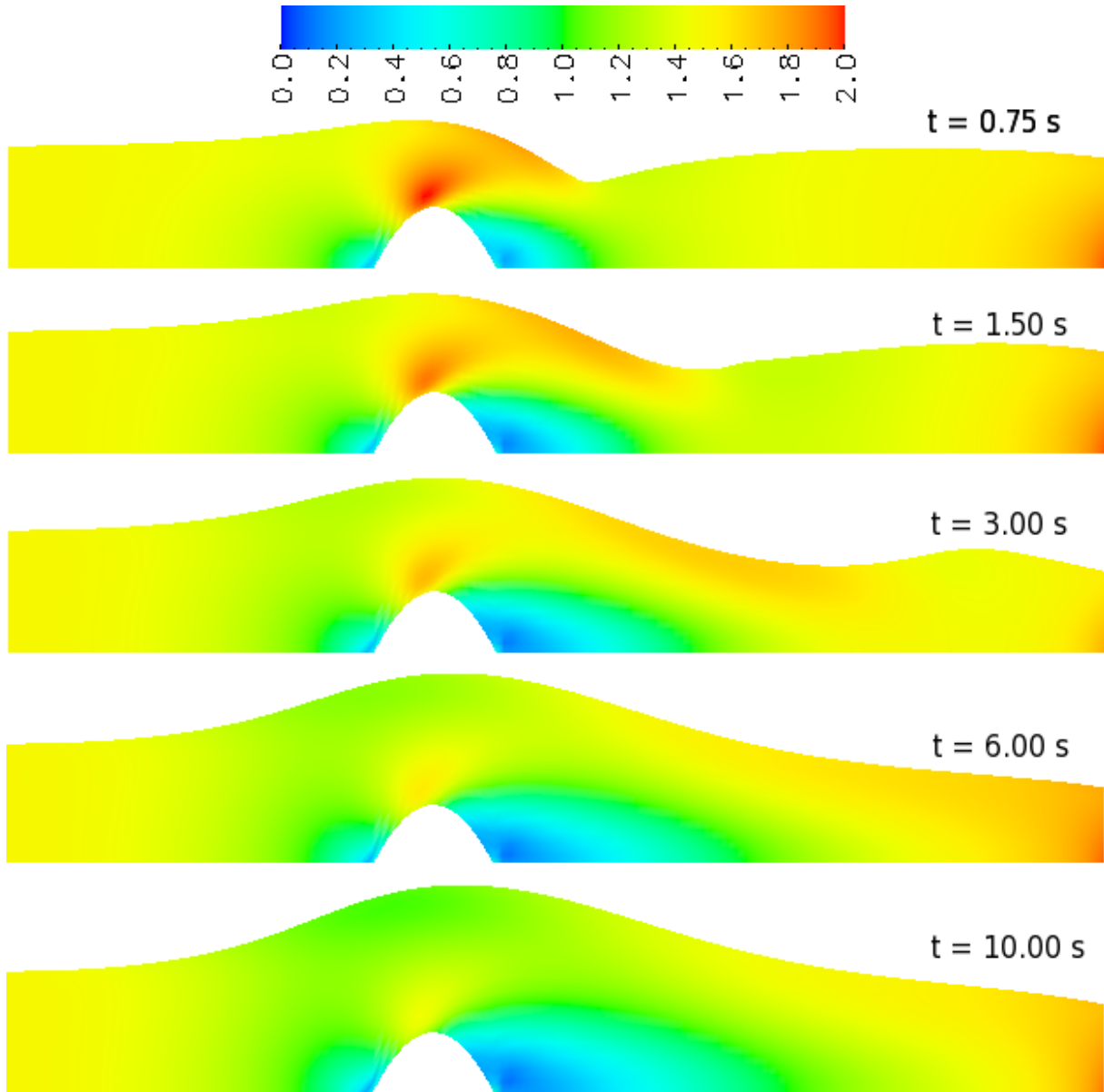


Figure 11: Free surface profile and absolute velocity values, in m/s, for the auxiliary problem with high viscosity ($\nu' = 0.05$ m²/s), for different times.

The simulation was made over a regular mesh of 15×135 quadrilateral elements and 2176 nodes. As in the beginning of the study there are violent free surface displacements due to the height of the obstacle and the mean flow velocity, an auxiliary analysis was made with $\nu' = 0.05$ m²/s and time step $\Delta t' = 0.01$ s along 1000 time steps, see Fig. 11. The objective of this first approach was obtaining a different initial position for the final study, that was made with the time step $\Delta t = 0.01$ s and the original viscosity value. All of the analyses were carried out with $\theta = 0.5$ and one prediction step, regarding the predominance of horizontal velocities over the vertical ones.

In spite of the character of an auxiliary result, the development of the profile of the free surface with higher viscosity and the evolution of the velocity field, also shown in Fig. 11, contribute with some interesting observations in comparison with the potential solution, such as the down waters displacement of the vertex of the free surface, probably originated by a kind of extension of the bump in the same direction produced by the low velocity sector. The peak height is of 1.70 m over the bottom of the channel, which is higher than the analogous potential problem solved in Forbes and Schwartz (1982).

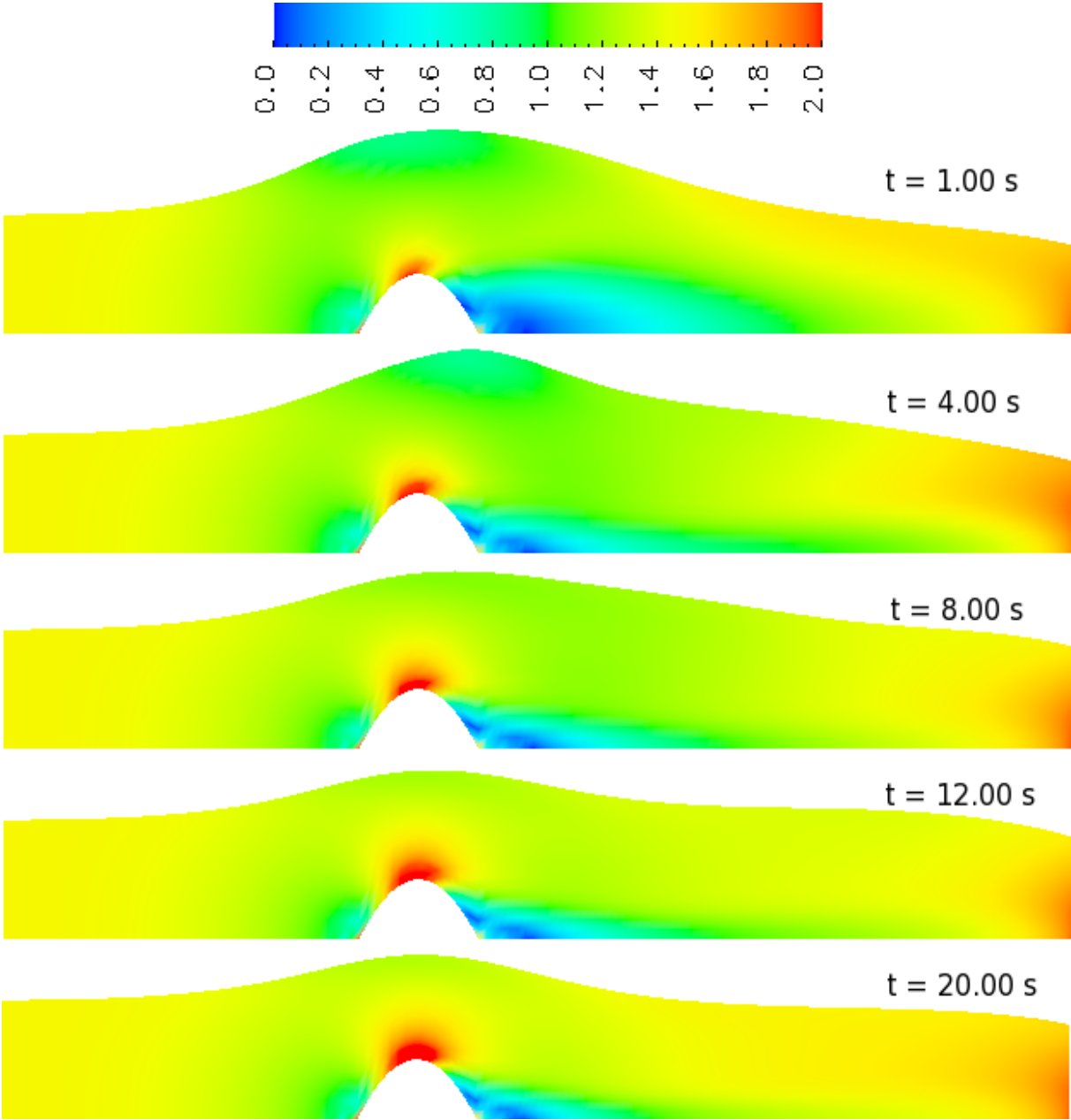


Figure 12: Free surface profile and absolute velocity values, in m/s, for the problem with $\nu = 0.005\text{ m}^2/\text{s}$, for five time steps.

The absolute velocity field and the evolution of the interface for the definitive value of ν , with $\Delta t = 0.01\text{ s}$ and for 2000 time steps, are plotted in Fig. 12. Unlike the more viscous analysis, the maximum profile height is lower, in this case of 1.38 m, and the vortex is practically centered

with the bump, giving an almost symmetric free surface profile, at least for the section closer to the bottom obstacle. Another difference with the former study is the maximum velocity position, which in this case is measured right over the bump instead the outlet section, while the low velocity sector down waters of the bump is smaller. The analysis gave a final state with quasi-stationary characteristics, i.e. very low variations in nodal positions and velocity values between consecutive states.

5 DISCUSSION

The wide range of performed tests allows the determination of the appropriate parameters to be used for different kind of problems, so far restricted to two-dimensional flows.

It was shown in Sec. 4.2 that one prediction step ensures mass conservation, e.g. an increment of less than 4% after 2000 time steps for $\theta = 0.5$ in the example. This situation was seen in other cases where horizontal velocities have stronger influence than vertical ones, like the supercritical flow considered in Sec. 4.3. Besides, the proposition of more prediction steps generates an increment of computational costs without leading to results of much higher quality, regarding either mass conservation or free surface displacements. From this point of view, a smaller time step would be more convenient than incrementing the prediction steps, and, even more, it is worth to test if some problems are well solved without any prediction step, as happened in the example presented in Sec. 4.1.

As in the case of the number of prediction steps used, the temporal integration should be also proposed as a function of the dominant velocity, i.e., a full implicit method when vertical velocity is larger than the horizontal one, or a semi-implicit one with $0.5 \leq \theta < 1$ for the opposite situation.

6 CONCLUSIONS

A free surface stabilization method was implemented and tested for two-dimensional problems as part of the PETSc-FEM library. Numerical tests were performed and its results were compared to reference solutions, showing good agreement between them, and consequently the consistence of the method. Nevertheless, there are some issues that should be solved in future work, like a deeper analysis of the intrinsic time τ_S influence, the parallel implementation of the code and the three-dimensional extension of the procedure.

Acknowledgments This work has received financial support from Consejo Nacional de Investigaciones Científicas y Técnicas (CONICET, Argentina, grants PIP 02552/00, PIP 5271/05), Universidad Nacional del Litoral (UNL, Argentina, grant CAI+D 2005-10-64) and Agencia Nacional de Promoción Científica y Tecnológica (ANPCyT, Argentina, grants PICT 12-14573/2003, PME 209/2003), and was partially performed with the *Free Software Foundation/GNU-Project* resources as GNU/Linux OS and GNU/Octave, as well as other Open Source resources as PETSc, MPICH and OpenDX.

REFERENCES

- Balay S., Buschelman K., Eijkhout V., Gropp W., Kaushik D., Knepley M., McInnes L., Smith B., and Zhang H. *Petsc 2.3.0 users manual*. Technical Report UC-405, Argonne Nat. Lab., 2005.
- Battaglia L., D'Elía J., Storti M.A., and Nigro N.M. Numerical simulation of transient free

- surface flows using a moving mesh technique. *Journal of Applied Mechanics*, 73(6):1017–1025, 2006a.
- Battaglia L., Franck G.J., Storti M.A., and D’Elía J. Numerical simulation of free-surface flows with volume control. In *Mecánica Computacional*, volume XXV, pages 169–183. 2006b.
- Behr M. and Abraham F. Free surface flow simulations in the presence of inclined walls. *Computer Methods in Applied Mechanics and Engineering*, 191(47-48):5467–5483, 2002.
- Brooks A.N. and Hughes T.J.R. Streamline upwind/Petrov-Galerkin formulations for convection dominated flows with particular emphasis on the incompressible Navier-Stokes equations. *Computer Methods in Applied Mechanics and Engineering*, 32:199–259, 1982.
- Donea J. and Huerta A. *Finite Element Methods for Flow Problems*. John Wiley & Sons, 2003.
- Forbes L.K. and Schwartz L.W. Free-surface flows over a semicircular obstruction. *Journal of Fluid Mechanics*, 144:299–314, 1982.
- García Espinosa J. *Un Método de Elementos Finitos para Análisis Hidrodinámico de Estructuras Navales*. Ph.D. thesis, Univerisdad Politécnica de Cataluña, 1999.
- Güler I., Behr M., and Tezduyar T. Parallel finite element computation of free-surface flows. *Computational Mechanics*, 23(2):117–123, 1999.
- Huerta A. and Liu W.K. Viscous flow with large free surface motion. *Computer Methods in Applied Mechanics and Engineering*, 69:277–324, 1988.
- Limache A. and Idelsohn S. Laplace form of navier-stokes equations: a safe path or a wrong way? In *Mecánica Computacional*, volume XXV, pages 151–168. 2006.
- López E.J., Nigro N.M., Storti M.A., and Toth J.A. A minimal element distortion strategy for computational mesh dynamics. *International Journal for Numerical Methods in Engineering*, 69(9):1898–1929, 2007.
- Message Passing Interface (MPI). 2006. <http://www.mpi-forum.org/docs/docs.html>.
- Prosperetti A. Motion of two superposed viscous fluids. *Physic of Fluids*, 24(7):1217–1223, 1981.
- Shyy W., Udaykumar H.S., Rao M.M., and Smith R.W. *Computational Fluid Dynamics with Moving Boundaries*. Taylor and Francis, 1996.
- Sonzogni V., Yommi A., Nigro N., and Storti M. A parallel finite element program on a Beowulf Cluster. *Advances in Engineering Software*, 33:427–443, 2002.
- Soulaïmani A., Fortin M., Dhatt G., and Ouellet Y. Finite element simulation of two- and three-dimensional free surface flows. *Computer Methods in Applied Mechanics and Engineering*, 86(3):265–296, 1991.
- Stein K., Tezduyar T., and Benney R. Automatic mesh update with the solid-extension mesh moving technique. *Comput. Meth. Appl. Mech. Engrg.*, 192:2019–2032, 2004.
- Tezduyar T., Aliabadi S., Behr M., Johnson A., and Mittal S. Parallel finite-element computation of 3d flows. *Computer*, 26:27–36, 1993.
- Xu Z. and Accorsi M. Finite element mesh update methods for fluid-structure interaction simulation. *Finite Element in Analysis and Design*, 40:1259–1269, 2004.